




## Article

# Study on the Mechanical Behavior of Fluid–Solid Coupling in Shallow Buried Tunnels under Different Biased Terrain

Hongsheng Qiu <sup>1</sup>, Ruihan Qiu <sup>2,\*</sup>, Gang Luo <sup>1,\*</sup> , Mo'men Ayasrah <sup>3,4,\*</sup>  and Zhe Wang <sup>1</sup> 

<sup>1</sup> School of Transportation and Logistics Engineering, Wuhan University of Technology, Wuhan 430063, China; 2755@whut.edu.cn (H.Q.); zhewang1001@whut.edu.cn (Z.W.)

<sup>2</sup> School of Urban Design, Wuhan University, Wuhan 430200, China

<sup>3</sup> Communication and Transportation Engineering, School of Transportation, Wuhan University of Technology, Wuhan 430063, China

<sup>4</sup> Department of Civil Engineering, Faculty of Engineering, Al Al-Bayt University, Mafrq 25113, Jordan

\* Correspondence: yukiQIU2019@outlook.com (R.Q.); luogang1997@whut.edu.cn (G.L.); ayasrahmomen@whut.edu.cn (M.A.)

**Abstract:** In the construction of mountain tunnels, biased and water-rich strata are often encountered. During tunnel excavation, the fluid–solid coupling has a great influence on the stability of the surrounding rock. This effect will be more severe when the terrain is biased. The bias tunnel points out the asymmetric load of the rocks which are surrounding the tunnels through the drilling or construction process due to the topographic situation. These loads can cause inverse actions during tunnel construction. Therefore, the effect of fluid–solid coupling on the displacement field, stress field, and seepage field of the tunnel surrounding rock under different biased terrains are studied in this paper. In the context of the Youzishu tunnel project, the numerical model is established to define the degree of terrain bias. Besides, the concept of bias coefficient is introduced. To achieve what is needed, 10 sets of increasing bias coefficients are obtained, by changing the inclination of the terrain to study the influence of formation bias degree on tunnel excavation in water-rich formations. After an in-depth analysis of the simulation results, it is found that the influence of fluid–structure interaction cannot be ignored. By analyzing ten groups of data under different working conditions, the biased terrain will aggravate this effect. As far as the displacement field of the surrounding rock is concerned, the biased formation has a greater impact on the deeply buried side than on the shallow-buried side, and has a greater impact on the vault than on the arch bottom. In addition, by analyzing the stress field and seepage field of the surrounding rock, a similar result can be obtained: the influence of formation bias on the deeply buried side is greater than that on the shallow-buried side, and the biased terrain will increase the pore pressure outside the tunnel lining and increase the water inflow. Finally, the locations where the displacement, stress, water pressure, and water inflow are the largest during the tunnel excavation process are found by the simulations and analyzed. Thus, attention can be paid to these locations, permitting a focus on protection during the construction process.

**Keywords:** tunnel; fluid–solid coupling; mechanical behavior; bias terrain; numerical simulation



**Citation:** Qiu, H.; Qiu, R.; Luo, G.; Ayasrah, M.; Wang, Z. Study on the Mechanical Behavior of Fluid–Solid Coupling in Shallow Buried Tunnels under Different Biased Terrain. *Symmetry* **2022**, *14*, 1339. <https://doi.org/10.3390/sym14071339>

Academic Editor: Sergei Alexandrov

Received: 24 May 2022

Accepted: 22 June 2022

Published: 29 June 2022

**Publisher's Note:** MDPI stays neutral with regard to jurisdictional claims in published maps and institutional affiliations.



**Copyright:** © 2022 by the authors. Licensee MDPI, Basel, Switzerland. This article is an open access article distributed under the terms and conditions of the Creative Commons Attribution (CC BY) license (<https://creativecommons.org/licenses/by/4.0/>).

## 1. Introduction

In light of the rapid urban development of major cities, the demand for solving traffic congestion problems is increasing. Recently, there has been an increasing trend in the number of mountain tunnels in China. However, in the construction of mountain tunnels, various complex strata are often encountered. Shallow bias tunnels commonly occur at mountainsides, tunnel entrances, and valley areas. Asymmetric surrounding rock pressure is exerted on the tunnel support system, resulting in asymmetric deformation and the potential for cracks and other risks, such as collapse and cracked linings. Thus, the bias tunnels point out the asymmetric load of the rocks which are surrounding the tunnels through the drilling or construction process, due to the topographic difference between

the left-hand and right-hand sides of the upper part of the tunnel. These asymmetric loads can have an inverse action during tunnel construction. Moreover, when the excavated strata are rich in groundwater, this adverse effect will increase, which will seriously affect construction safety. Therefore, the excavation of the tunnel should be handled with care when the eccentric terrain and the water-rich strata exist at the same time [1].

At present, the investigation of bias tunnels principally concentrates on several approaches, such as field monitoring, numerical modelling, and theoretical methods. Furthermore, the research on bias tunnels is mainly to simulate practical engineering, analyze the stress and displacement trend of the surrounding rock during the excavation process, as well as the control and prediction of the surface subsidence, and the mechanical and construction stability of the surrounding rock [1–12]. In addition, in relation to the judgment about, and classification of, biased tunnels, “Highway Tunnels and Technical Specifications” (JTG/T3660-2020) gives an authoritative explanation [13]. On this basis, according to the stress characteristics of the tunnel-surrounding rock, the bias coefficient is defined, which can quantify the bias degree of the terrain more accurately [14]. In addition, the influence of the different stratum dip angles on the displacement, stress, and surface subsidence of the surrounding rock of the tunnel has a reference value for engineering [15–17].

Under water-rich conditions, it is necessary to consider fluid–solid coupling in the simulation of the tunnel excavation. Not only should the influence of the seepage force on the stability of surrounding rock be considered [18–21], but also the water pressure at key locations should be monitored, and the water inflow of the tunnel should be predicted, to deal with the possible water seepage and water inrush in the tunnel in advance, and to ensure construction safety [22–28].

Lee et al. [29] proposed a simplified elastoplastic analytical solution for the displacement and stress of a circular tunnel in the soft rock under steady seepage, and its accuracy was verified by numerical analysis. In addition, a semi-analytical method was proposed for a tunnel crossing an inclined aquifer by Hwang et al. [30], and the water gushing and water level drop caused by the tunnel excavation were evaluated.

With that in mind, the theoretical analytical solutions of fluid–structure interactions in tunnels are complicated and have specific, ideal assumption conditions, which are not suitable for practical projects in various complicated situations. Thus, the appearance of the numerical modelling solves this problem very well.

In this way, several studies based on numerical modeling, especially the finite difference method, have been presented to simulate tunnel excavation and have been widely used in the field of geotechnical engineering, since it is capable of providing detailed insights into physical quantities, such as displacements, velocities, stresses, plastic strains, flow rates at every spatiotemporal solution time step [31,32].

According to the full numerical simulation, the modeling analysis conducted by Yang et al. [33] carried out a 3D finite difference method to study the soft rock tunnel construction in different sections and analyzed the surrounding rock deformation and the plastic area size and distribution.

In the same line, the authors of [34] executed three-dimensional finite-difference analyses to investigate the effect of the mechanical properties of the surrounding rock mass and bench length on the stability of the tunnel. The results showed that the deformation of the tunnel is small when the modulus of the elasticity of the rock mass reaches a certain value, in the case of shallow-buried and large cross-section tunnels.

However, when the strata have both biased terrain and rich water, the stability of the surrounding rock will be greatly threatened, and the dangerous situation of water seepage and water inrush is more likely to occur. The strata where the Youzishu Tunnel is located have both bias and water-rich conditions. Therefore, the aim of this research is to study the effect of fluid–solid coupling on the displacement, stress, and seepage fields of the Youzishu tunnel-surrounding rock under different bias terrain, using the FLAC3D numerical program [35]. The obtained results can be applied in practical engineering.

## 2. Case Study

### 2.1. The Khufu Bypass Highway Project in Xingshan County

As shown in Figures 1 and 2, The Public—Private partnership engineering of the reconstruction of Khufu, Wang Zhaojun, and S287 Orchard-Shuiyuesi roads in Xingshan County is 42.172 km long. The G209 Xingshan County Gough Beltway is 11.541 km long, with 10 bridges of about 1460 m and three tunnels of about 3260 m. The width of the roadbed is 8.5 m, and the design speed is 40 km/h. Figures 1 and 2 show the G209 route map of the Khufu roundabout in Xingshan County and the G209 topography and landform around the Khufu Bypass road project in Xingshan County. The project area is part of the Qin Mountains/Daba Mountains system, with mountains extending from east to west. The total terrain is high on three sides, low on the south, and rising gradually from south to north. G209 Xingshan County's Khufu circuit runs along the eastern bank of the Khufu River.



Figure 1. G209 route map of Khufu roundabout in Xingshan County.



Figure 2. G209 topography and landform around the Khufu Bypass road project in Xingshan County.

### 2.2. Soil Conditions

Currently, the support parameters design of the highway tunnels in China is fundamentally based on the surrounding rocks' grade [36]. The categorization of the grade of the surrounding rocks depends on a number of factors, such as rock integrity and hardness,

structural plane, and groundwater. However, the total length of the Youzishu tunnel is 1906 m, including 1476 m in the Grade V section, 370 m in the Grade IV section, 60 m in the Fracture Zone, and 1254.3 m<sup>3</sup>/d in normal water inflow. The net width and net height of the main tunnel are 11.5 m and 9.75 m, respectively. The slope and the side of the tunnel entrance are unstable structures, and there is a risk of collapse during construction. The silty clay and crushed stone soil cover the entrance and exit of the tunnel, the soft rock is the main surrounding rock in the cave body, and it is easy for it to collapse and experience water gush under bad geological conditions.

Based on the site investigation reports, the surrounding rock of the tunnel is of Grade V. The terrain condition is shallow buried, and biased, taking into account the groundwater seepage, but not taking into account the fractured zone and other complex conditions. According to the site conditions, the ground inclination angle of the selected section is simplified to 9°, which is in good agreement with the engineering practice.

### 3. Numerical Analysis Modelling

#### 3.1. Set Condition

The method is proposed to determine the degree of unsymmetrical pressure in the tunnel under unsymmetrical topography, that is, the unsymmetrical coefficient of the load on both sides of a deeply buried tunnel is defined according to Equation (1) [13]:

$$C_{un} = \frac{q_s - q_q}{\frac{1}{2}(q_s + q_q)} = \frac{2 \tan \alpha B^2}{(2h - B \tan \alpha)2B - (\lambda h^2 + \lambda' h'^2) \tan \theta} \quad (1)$$

where,  $q_s$  to describe the deeply buried side load;  $q_q$  to describe the shallow-buried side load. The  $C_{un}$  value is in the range of 0~2; the larger the  $C_{un}$  value is, the greater the terrain bias is;  $h$  and  $h'$  are the height from the level of the vault to the ground ( $h$  for the deeply buried side while  $h'$  for the shallow-buried side);  $B$  is the excavation span;  $\gamma$  to describes the weight of the surrounding rock (kN/m<sup>-3</sup>);  $\theta$  is the friction angle (°) on both sides of the topsoil column;  $\alpha$  is the inclination of the ground.  $\lambda$  and  $\lambda'$  are the lateral pressure coefficients of the inner and outer sides, respectively. In addition, Figure 3 presents the sketch map of the surrounding rock pressure of the tunnel. In addition, ten models were built by rotating ten straight lines around the same point at a certain angle, to obtain ten different ground inclinations. Therefore, Figure 4 shows the models under different terrain inclinations and settlement monitoring points, while Table 1 presents the value of the bias coefficient under different terrain inclinations. It is worth mentioning that, based on the topography and the axis of the tunnel center, the tunnel is divided into shallow and deep sides. Hence, the bias coefficient represents the asymmetry of the surrounding rock stress on the lining of the shallow and deep sides.

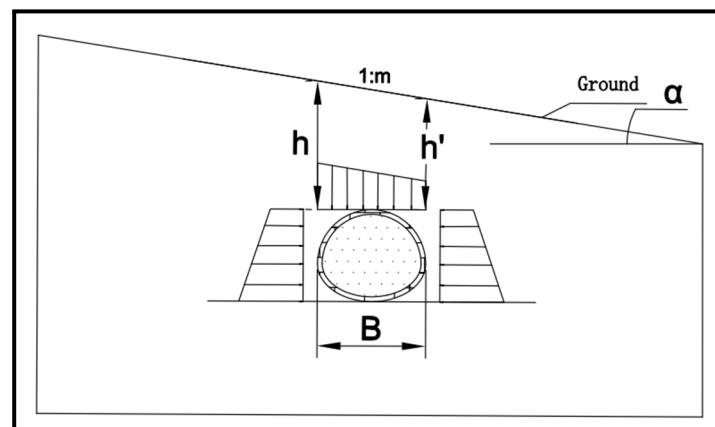


Figure 3. Sketch map of surrounding rock pressure of tunnel.

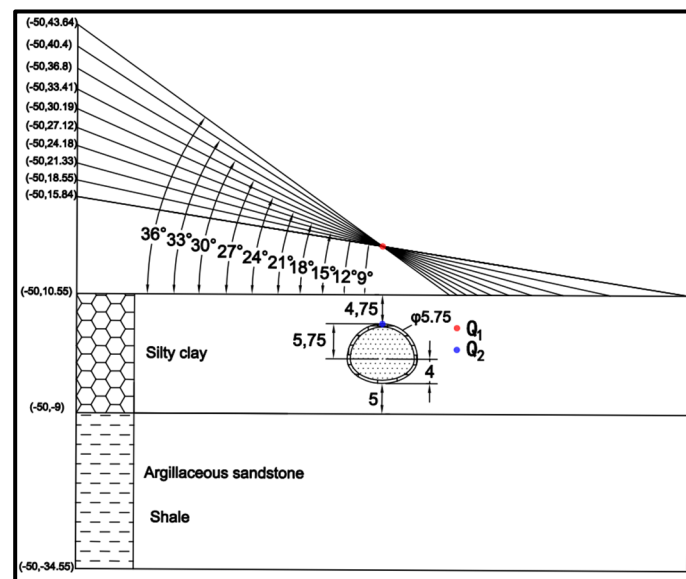


Figure 4. Models under different terrain inclinations and settlement monitoring points ( $Q_1$  and  $Q_2$ ).

Table 1. The value of bias coefficient under different terrain inclination.

Group	$\alpha$ ( $^{\circ}$ )	h (m)	h' (m)	Bias Coefficient (-)
1	9	13.58	11.76	0.2
2	12	13.91	11.46	0.27
3	15	14.22	11.14	0.35
4	18	14.55	10.81	0.43
5	21	14.89	10.47	0.53
6	24	15.24	10.13	0.63
7	27	15.61	9.75	0.76
8	30	16.00	9.37	0.90
9	33	16.42	8.95	1.06
10	36	16.49	8.18	1.23

### 3.2. Numerical Model and Boundary Condition

The model is located in a section near the exit of the tunnel, where the geological topography is shallow and rich in water, the surrounding rock is soft, and there are fault fracture zones, which are prone to collapse and water and mud gushing. Figure 5 shows the developed 3D model using FLAC3D. The mesh used in this model consists of 50,251 nodes and 47,040 elements. The dimensions of the model are 100 m in the transverse direction and 60 m in the vertical direction, that is, the calculation boundary of the left and right sides is four times the total tunnel span, the calculation boundary of the lower side is three times the total tunnel height, and the excavation depth is three times the tunnel diameter, that is 30 m. In the vertical direction, the deep side is 60 m, the shallow side is 45 m, and the left-high right-low bias terrain is formed. The tunnel's buried depth is 12 m, which is a shallow tunnel. Therefore, these dimensions are sufficiently large to eliminate the effect of boundary conditions on the numerical results, because the massive raise in the stratum size does not lead to any change in the analysis results. In this model, the boundary conditions are set as follows: the top side is a free surface; the four side surfaces restrain its normal displacement; and the bottom surface restrains the displacement in three directions. In this model, the shell element is used for the initial support, and the groundwater seepage

is considered, the groundwater level is parallel to the mountain terrain, the groundwater level is set by the water table, and the tunnel excavation and lining are considered to be impermeable structures.

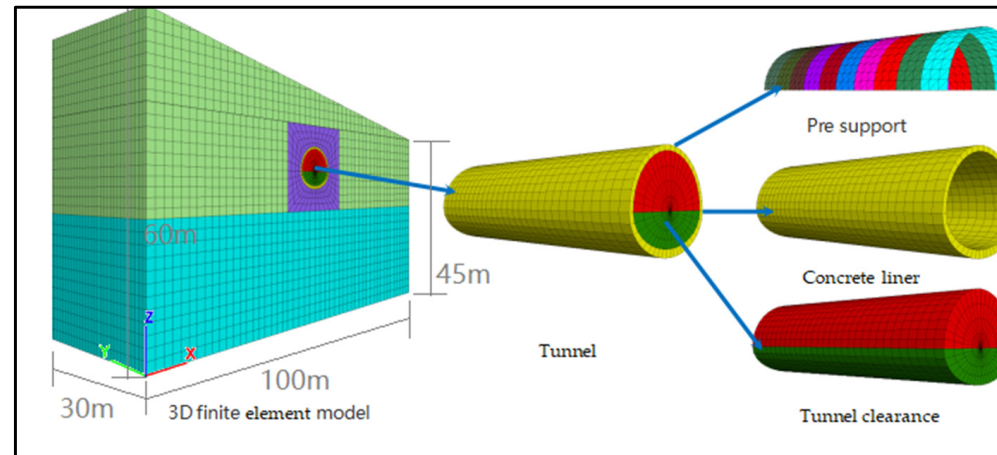


**Figure 5.** 3D numerical simulation.

### 3.3. Constitutive Models and Material Parameters

In the numerical calculation of FLAC3D, the mechanical model of the material is based on the elastic, perfectly plastic Mohr–Coulomb model, while the elastic model is used for the concrete tunnel lining. The model has two strata, the first layer is mainly silty clay and is judged to be Grade V surrounding rock with a thickness of 24.84 m (For group 1), and the second layer is mainly argillaceous sandstone and shale, which is determined to be Grade IV surrounding rock, and its thickness is 25.55 m. The parameters of Bulk Modulus ( $K_1$ ), Poisson's ratio ( $\nu$ ), cohesion ( $C$ ), and Friction angle ( $\theta$ ) are defined. The Bulk Modulus ( $K_1$ ), Elastic Modulus ( $E$ ), and Shear Modulus ( $G$ ) can be converted by Poisson's ratio ( $\nu$ ) as the following equations [35]:

$$K_1 = \frac{E}{3(1-2\nu)} \quad (2)$$

$$G = \frac{E}{2(1+\nu)} \quad (3)$$

It is worth mentioning that, when calculating the fluid–solid coupling effect of rock and soil mass, the rock mass should be regarded as a porous medium. The flow of fluid in the porous medium is based on Darcy's law and Biot's equation, additional parameters, such as porosity and permeability of the material, are defined. There are four types of seepage boundary conditions to choose the fluid–solid coupling model, including the given pore water pressure, the given normal flow rate outside the boundary, the permeable boundary, and the impervious boundary. In the analysis process, the mechanical calculation time is much longer than the coupling diffusion time, so a single seepage analysis, that is, a drainage analysis, can be performed. It is well-acknowledged that the soil is considered an incompressible granular material. The parameters involved are Permeability Coefficient ( $K_2$ ), Density of Water ( $\rho_f$ ), Gravity ( $g$ ), Biot Coefficient ( $\alpha_B$ ), Bulk Modulus ( $K_1$ ) and porosity ( $\mu$ ). In this case, the Permeability Coefficient is of the same nature as the Pressure Coefficient in Darcy's law, and is related to the Hydraulic Conductivity ( $K_h$ ), using Equation (4) [35]:

$$K_2 = \frac{K_h}{\rho_f g} \quad (4)$$

The ratio of fluid–solid stiffness ( $R_k$ ) plays an important role in the analysis of fluid–solid coupling problems. According to the numerical value of the fluid–solid stiffness ratio, the fluid–solid coupling problems can be divided into relatively rigid skeleton problems and flexible skeleton problems. In this case, the model is a relatively flexible skeleton:

$$R_k = \frac{\alpha_B^2 M}{k_1 + 4G/3} \quad (5)$$

where  $M$  is Fluid Modulus;  $K_1$  is Bulk Modulus;  $G$  is Shear Modulus; and  $\alpha_B$  is the Biot Coefficient [35].

According to the geological investigation reports, the soil layers and materials' engineering properties and the groundwater seepage calculation parameters are given in Tables 2 and 3, respectively.

**Table 2.** Soil layers and materials engineering parameters.

Soil and Materials	Bulk Modulus (GPa)	Poisson's Ratio (–)	Density (kg/m <sup>3</sup> )	Cohesion (MPa)	Friction Angle (°)
Grade V surrounding rock	0.05	0.3	2000	0.2	14
Grade IV surrounding rock	0.42	0.25	2250	0.23	22
Pre-support	21.0	0.2	-	-	-
Concrete liner	11.5	0.2	2200	-	-

**Table 3.** Groundwater seepage calculation parameters.

Soil Layers	Porosity (–)	Permeability (cm·s <sup>−1</sup> )	Void Ratio (–)	Penetration (m <sup>2</sup> ·Pa <sup>−1</sup> ·s <sup>−1</sup> )
Grade V surrounding rock	0.7	$1.4 \times 10^2$	0.41	$1.4 \times 10^{10}$
Grade IV surrounding rock	0.65	$9 \times 10^3$	0.39	$9 \times 10^{11}$

### 3.4. Numerical Analysis Procedure

The selected section of this model is shallow buried and unsymmetrical topography, the normal water inflow is 1254.3 m<sup>3</sup>/d, the surrounding rock is soft rock. Stratum 1 is mainly silty clay, crushed rock, and block rock, and the surrounding rock is Grade V; stratum 2 is mainly argillaceous sandstone, shale, and Grade IV surrounding rock. According to the above construction schedule, the Grade V surrounding rock section is excavated 1.5 m per day, and the second lining is started two months after the construction. To reduce the model grid and speed up the calculation, the method of micro-step is chosen when the model is built, namely, excavate 3 m per day and take 3 m from the excavation footage. Figure 6 shows the tunnel construction flowchart, and the model is simplified in the following construction steps:

- (1) generating initial stress field and seepage field;
- (2) synchronously excavating up and down steps;
- (3) carrying out initial support for up steps;
- (4) set fluid on, set mechanical off, set seepage time, carry out seepage calculation;
- (5) set mechanical on, set fluid off, solving;
- (6) full-section lining.

Then, steps four and five are repeated. In accordance with the above construction steps, the excavation cycle is 10 m footage, each footage for 3 m.

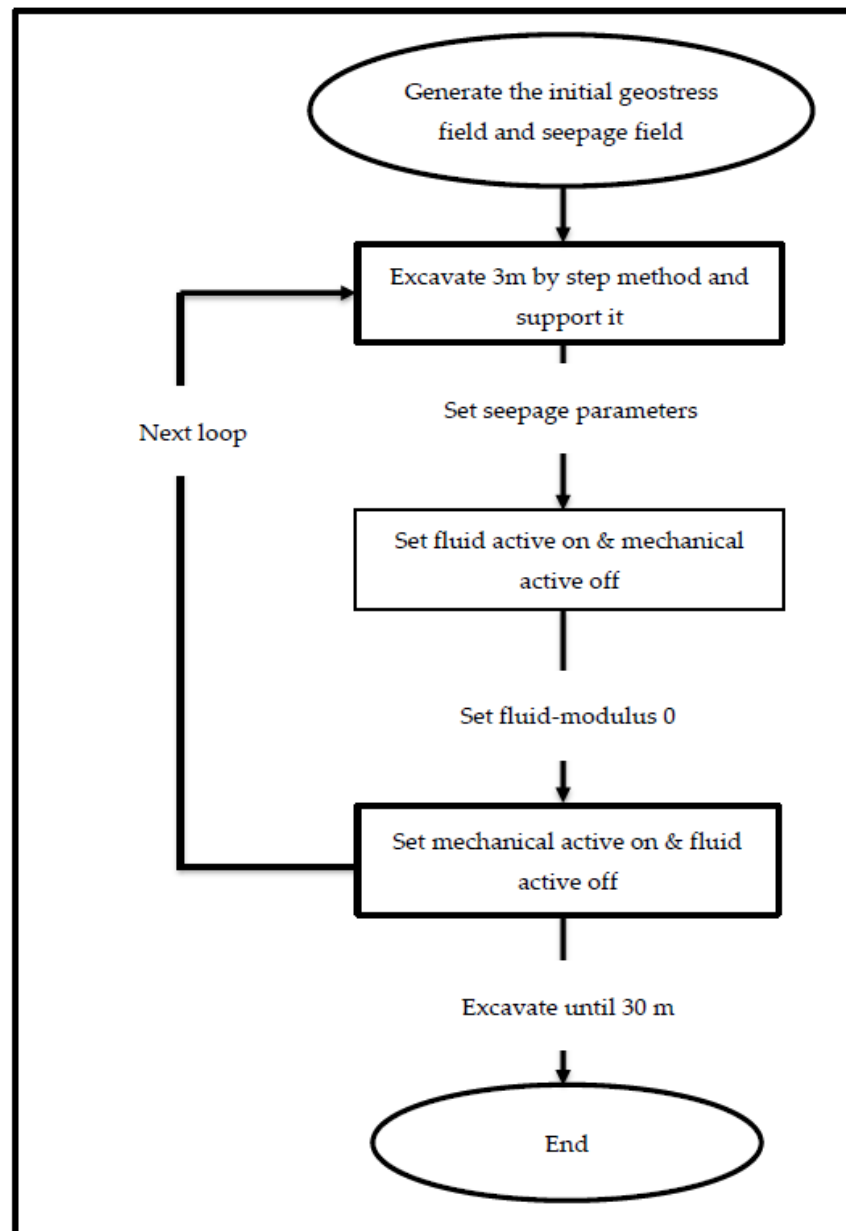


Figure 6. Tunnel construction flowchart.

#### 4. Verification of the Numerical Model

To assess the capability of the calculation results and verify the validity of the 3D model, it is vital to compare the field measurements with the settlement values of the monitoring points in the simulation calculation results. Therefore, there are four site monitoring points ( $Q_1-0$ ,  $Q_1-15$ ,  $Q_2-0$ ,  $Q_2-15$ ), points  $Q_1-0$  and  $Q_1-15$  are the monitoring points at the tunnel section depth of 0 m and 15 m, which monitor the longitudinal settlements of the surface. Meanwhile points  $Q_2-0$  and  $Q_2-15$  are the monitoring points at the tunnel section depths of 0 m and 15 m, which monitor the longitudinal settlements of the tunnel vault.

Figures 7 and 8 show the comparison curves between the values of the numerical simulation and the actual monitoring values. The comparisons have indicated a good agreement between the numerical modelling and the measured values, and the simulation results are in line with the actual engineering.



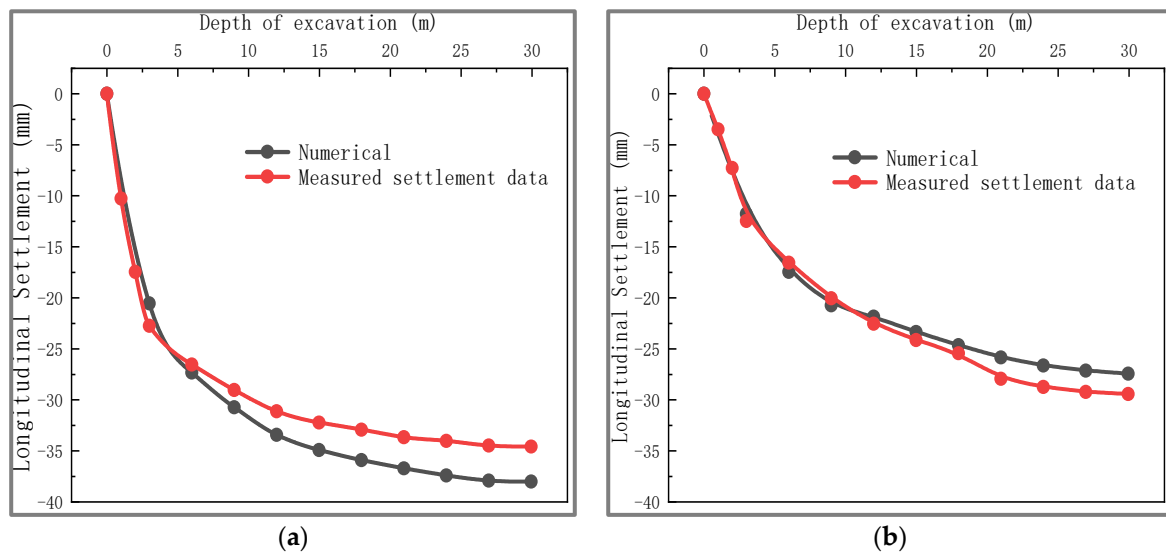


Figure 7. The longitudinal settlement of points (a)  $Q_1-0$  and (b)  $Q_2-0$ .

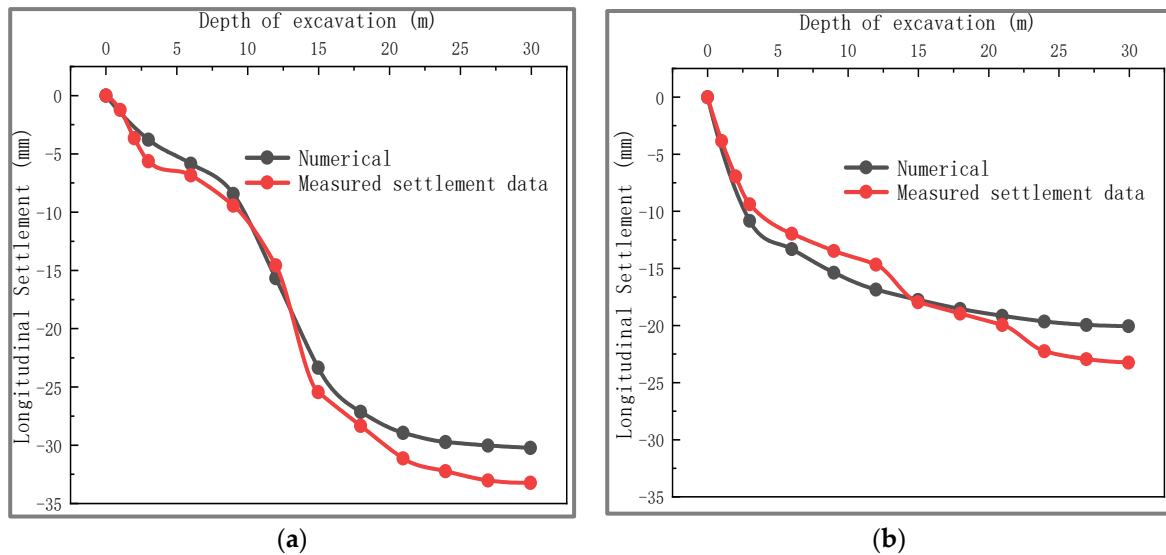


Figure 8. The longitudinal settlement of points (a)  $Q_1-15$  and (b)  $Q_2-15$ .

On the other hand, as shown in Figure 7, the vault settlement is higher than the surface settlement on the same tunnel section depth. In addition, the longitudinal settlement of  $Q_1-15$  has a mutation at the depth of 15 m, which indicates that the vault settlement increases greatly under the excavation of the palm surface, as shown in Figure 8.

## 5. Results

### 5.1. Influence of Groundwater Seepage on the Longitudinal Settlement of Surrounding Rock of the Tunnel

Two monitoring points,  $Q_1-0$  and  $Q_2-0$ , were selected to discuss the variation law of tunnel vault and surface settlement under different biased terrains. The vault settlement at the same monitoring point is greater than the surface settlement, which is the result obtained after tunnel excavation and support, because tunnel excavation has greater disturbance to the vault.

On the other hand, when the fluid–structure interaction is not considered, as shown in Figure 9, with the increase in the bias angle, the vault settlement increases by 16.7%, and the surface subsidence increases by 15.8%, which indicates that the bias angle has a great

influence on the disturbance of the surrounding rock of the tunnel and the impact on the vault is slightly greater than the surface.

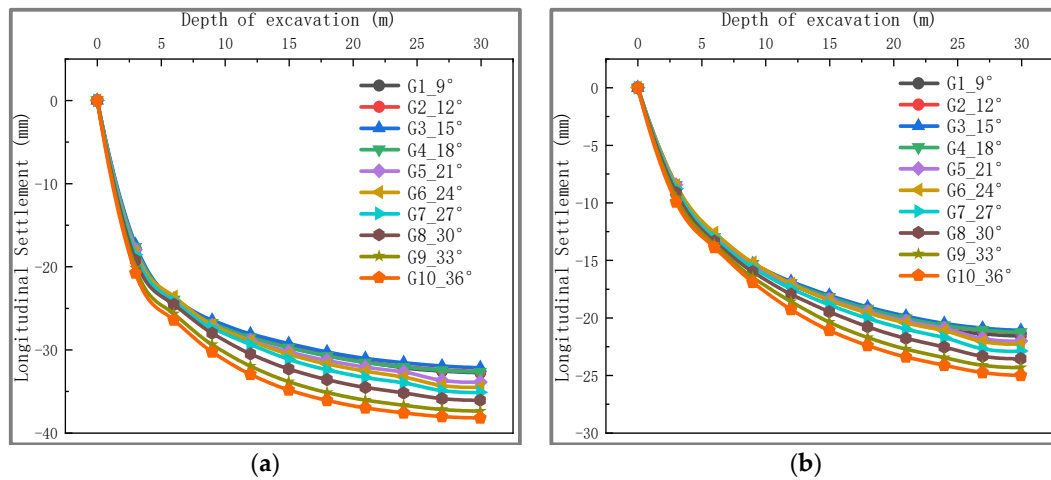


**Figure 9.** The longitudinal settlement under 10 different terrains when fluid–structure interaction is not considered for (a) Q1-0; (b) Q2-0.

Otherwise, when considering the fluid–structure interaction, as shown in Figure 10, the vault subsidence increases by 15.5%, and the surface subsidence increases by 28.4%, which indicates that when the groundwater is considered, the influence of the bias angle on the surface is greater than that of the vault.

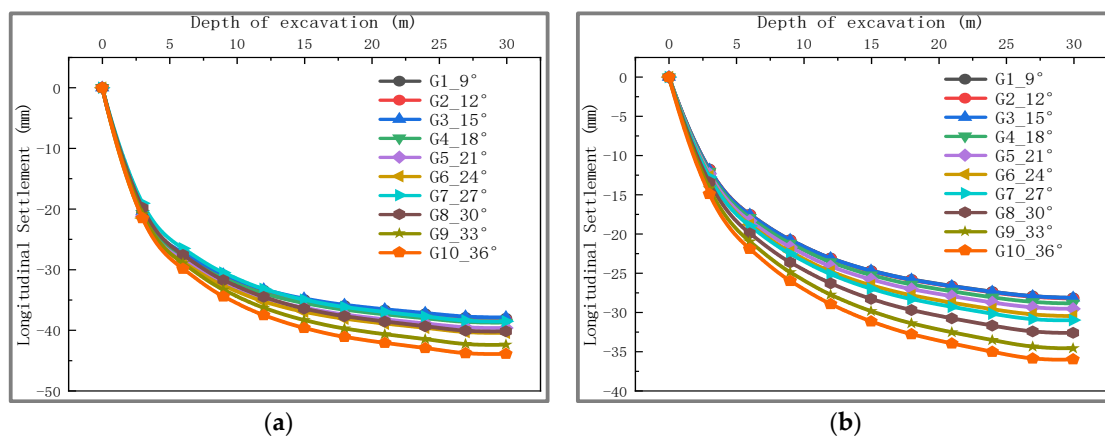


**Figure 10.** The longitudinal settlement under 10 different terrains when fluid–structure interaction is considered for (a) Q1-0; (b) Q2-0.

Finally, it can be concluded that, under the action of fluid–solid coupling, the increase in the bias angle has a particularly obvious effect on the surface settlement. Therefore, when there is a situation of shallow burial and large bias, more attention should be paid to the protection of the soil at the surface to avoid preventing slippage, collapse, and other dangerous situations.

## 5.2. Influence of Bias Terrain on the Mechanical Behavior of Surrounding Rock of Tunnel

### 5.2.1. Horizontal Displacement and Vertical Displacement

The data selected in Figure 11 are the maximum horizontal and vertical displacement of the same section. By comparison, the results indicate that the maximum horizontal displacement that occurs at the deep-buried side is larger than on the shallow-buried side. When the bias coefficient increases from 0.2 to 1.23, the horizontal displacement of the deeply buried and shallow-buried sides increases by 58.6% and 68.5%, respectively.

In addition, it shows that the change of the bias coefficient has a great influence on the horizontal displacement of the deeply buried side. In terms of vertical displacement, the maximum settlement occurs on the deeply buried side of the vault, and the maximum uplift occurs on the shallower buried side of the arch bottom. With the increase in the bias coefficient, the maximum settlement of the vault increased by 46%, and the maximum uplift of the vault increased by 12.4%. Again, it shows that the change of the bias coefficient has a great influence on the settlement of the vault.

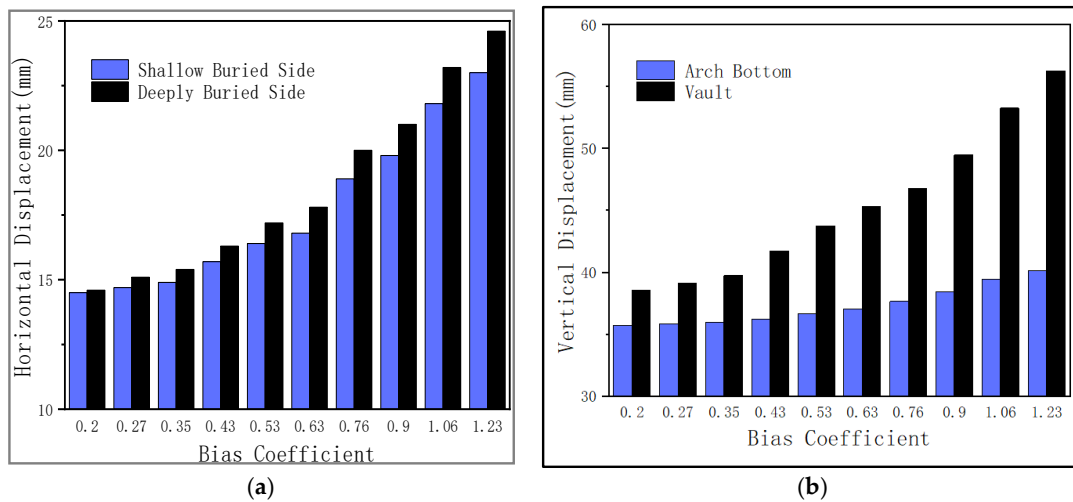


**Figure 11.** (a) Maximum horizontal displacement (absolute value) of deeply buried side and shallow-buried side under 10 different bias coefficients; (b) Maximum vertical displacement (absolute value) of vault and arch bottom under 10 different Bias Coefficients.

To sum up, it can be concluded that the bias pressure will increase the effect of seepage on the displacement of the surrounding rock of the tunnel. More precisely, the impact on the deeply buried side is greater than that on the shallow-buried side, and the impact on the vault is greater than that on the bottom of the vault.

5.2.2. Huber–Von Mises Stress and Tensor Stress

Figure 12 shows the distribution of the equivalent stress of the tunnel-surrounding rock and the distribution of the principal stress. The green short line represents the intermediate principal stress tensor, the red line represents the maximum principal stress tensor, and the blue line represents the minimum principal stress tensor. These quantities can represent the failure criterion of the material; the larger the structure, the more unstable it is.

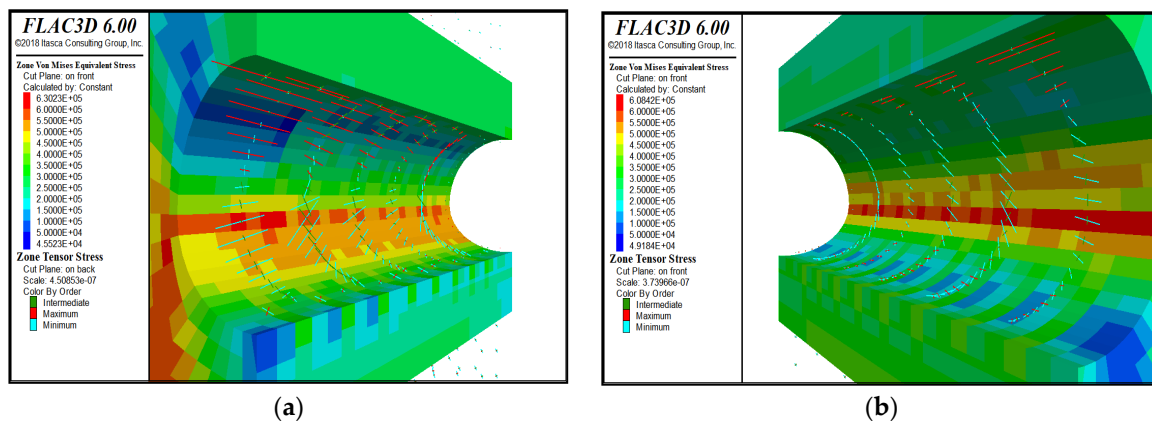


**Figure 12.** Numerical simulation results of Huber–von Mises stress and tensor stress for (a) deeply buried side; (b) shallow-buried side.

Figure 13 shows that, with the increase in the bias coefficient, the stress on the deeply buried side increases significantly. In particular, the maximum principal stress, which increased by 12.5%. On the other hand, the stress on the shallow-buried side does not change significantly. This shows that the increase in the bias coefficients will reduce the stability of the surrounding rock on the deeply buried side of the tunnel. Therefore, during excavation, special attention should be paid to the support of the deeply buried side.

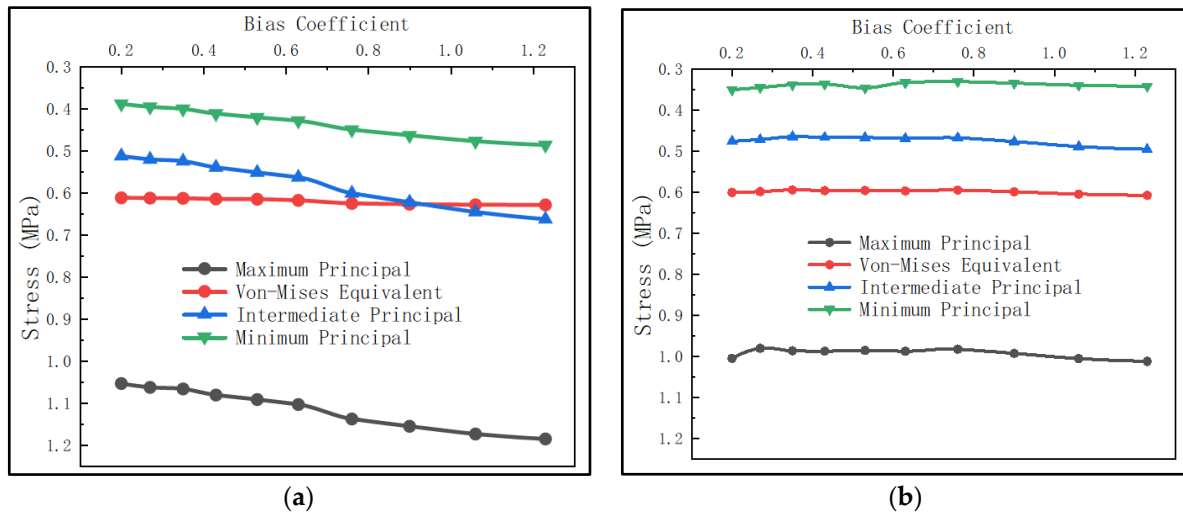


Figure 13. The maximum, intermediate, minimum principal stresses tensor, and Huber–von Mises stress under 10 different bias coefficients for (a) deeply buried side; (b) shallow-buried side.

### 5.3. Influence of Bias Terrain on the Seepage Behavior of Surrounding Rock of the Tunnel

#### 5.3.1. Flow Vectors

Figure 14 describes the distribution of Flow Vectors around the tunnel. It can be noted that the seepage vector distribution of the entire model, as well as the size and direction of the seepage vector around the tunnel, can be seen. In addition, it can be determined that the most likely location of the water seepage in the tunnel is at the arch waist on both sides, and that the deeply buried side arch waist is the most dangerous.

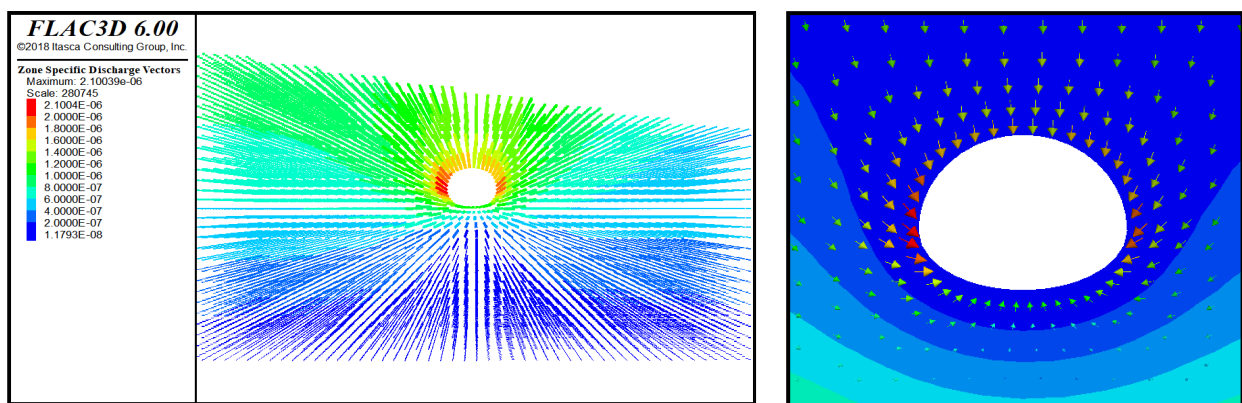


Figure 14. The distribution of flow vectors around the tunnel.

It can be seen from Figure 15 that, with the increase in the bias coefficient, the seepage vector on the deeply buried side increases significantly, increasing by 14.6%, while the shallow-buried side has no growth trend, but a slight decrease trend. Through the average seepage vector of the tunnel section, the water inflow per linear meter of the tunnel was calculated, and it was found that the water inflow changed significantly with the increase in the bias coefficient, and increased by 6%. It can be seen that the bias voltage has a

great influence on the seepage vector on the deeply buried side, and has a non-negligible influence on the water inflow of the tunnel.

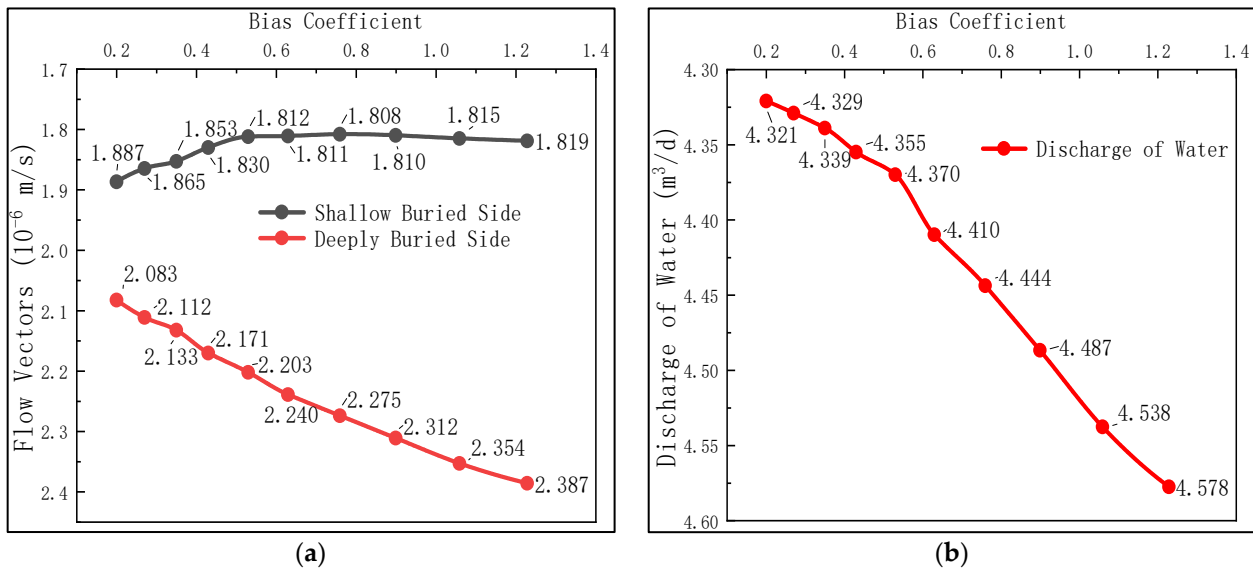


Figure 15. (a) The maximum flow vectors under 10 different bias coefficients for both shallow- and deep-buried sides; (b) The water flow in the tunnel per linear meter.

### 5.3.2. Pore Pressure Outside the Lining

Figure 16 shows the water pressure distribution outside the lining and the variation curve of the five monitoring points (A, B, C, D, and E) with the bias coefficient. It can be observed that the water pressure on the lining at the bottom of the vault is the largest, followed by the waist of the deeply buried side, and the top vault is the smallest. Compared with the other monitoring points, the bias coefficient has a greater influence on the external water pressure of the lining at the bottom of the arch and the deeply buried side. This also echoes the previous conclusions.

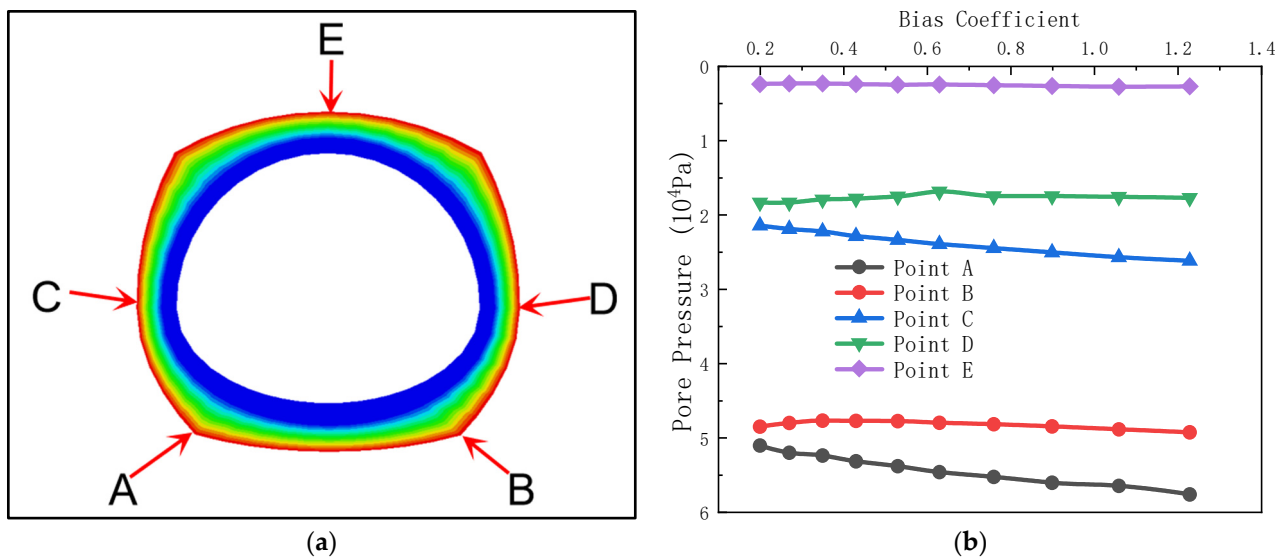


Figure 16. (a) The distribution of pore pressure outside the lining and monitoring points; (b) The values of pore pressure for monitoring points (A, B, C, D, and E) under 10 different bias coefficients.

## 6. Conclusions

Taking the Youzishu tunnel as the background, a series of 3D numerical models were carried out using FLAC3D software, and the concept of bias coefficient was introduced. The

mechanical behavior laws of tunnels under different biased strata are studied, including the displacement stress, and seepage fields. This study shows that the degree of formation bias has a great influence on the excavation of the tunnels in water-rich formations. After in-depth analysis, it was found that the influence of the fluid–structure interaction cannot be ignored. The main conclusions are as follows:

1. Through the analysis of the displacement field, the influence of bias pressure on the displacement of the deeply buried side is greater than that of the shallow-buried side, and the influence on the displacement of the vault is greater than that of the arch bottom; the bias coefficient has the greatest effect on the maximum principal stress;
2. In terms of the displacement field, the bias coefficient has the greatest effect on the maximum principal stress, which increased by 12.5%, so its impact on the stability of the tunnel cannot be ignored;
3. For the seepage field, the influence of bias pressure on the water pressure and seepage vector of the deeply buried side is greater than that of the shallow-buried side. In addition, the bias pressure will increase the water pressure outside the tunnel lining and the water inflow volume of the tunnel, and the most likely place for water seepage is at the left arch waist;
4. Based on the influence of different bias degrees on the displacement field, stress field, and seepage field, it can be concluded that, under the action of fluid–solid coupling, the influence of formation bias on the deeply buried side is greater than that on the shallow-buried side, and the larger the bias coefficient, the more serious is the situation. Therefore, in the construction of large-biased shallow-buried water-rich tunnels, attention should be paid to the protection of the deep-buried side of the tunnels.

**Author Contributions:** Conceptualization, H.Q., G.L., M.A., R.Q. and Z.W.; formal analysis, M.A., R.Q. and G.L.; investigation, H.Q., G.L., R.Q. and M.A.; writing—original draft preparation, M.A., G.L. and H.Q.; supervision, H.Q. All authors have read and agreed to the published version of the manuscript.

**Funding:** The publishing of this paper is financially supported by the National Natural Science Foundation of China (No. 11672215).

**Institutional Review Board Statement:** Not applicable.

**Informed Consent Statement:** Not applicable.

**Data Availability Statement:** The data presented in this study are available on request from the corresponding author.

**Conflicts of Interest:** The authors declare no conflict of interest.

## References

1. Zhang, C.; Wang, C.; Niu, X.; Zhang, S.; Zhao, H. Effect of the Double-Line Spiral Tunnel Curvature on the Tunnel Construction Stability. *Adv. Civ. Eng.* **2020**, *2020*, 1–9. [[CrossRef](#)]
2. Zhang, G.; Liu, H.B. The Simulation Analysis of Large Cross-Section Soft Rock Tunnel Excavation under the Bias Terrain. In *Applied Mechanics and Materials*; Trans Tech Publications Ltd.: Zurich, Switzerland, 2011; Volume 90, pp. 1853–1858.
3. Li, W.H.; Peng, L.M.; Lei, M.F.; An, Y.L. Secondary and primary stress distribution of terrain bias tunnel. *Railw. Eng. Sci.* **2012**, *4*, 63–69.
4. Dong, J.-H.; Xie, Y.-B.; Li, J.-J.; Kou, H.-J.; Zhao, Y.-D. New Protective Structure for Shallow-buried Bias Tunnel at Portal Section and Its Simplified Calculation Method. *China J. Highw. Transp.* **2018**, *31*, 339.
5. Xiaohong, G.A.N.; Liping, C.H.E.N.; Sulei, Z.H.A.N.G. On law of ground settlements and its prediction method for the shallow-buried tunnel under asymmetrical pressures. *Mod. Tunn. Technol.* **2019**, *56*, 78–84.
6. Fu, H.L.; Li, J.; Wang, H.T.; Zhang, J.B.; Huang, Z. Research on the ground settlement prediction in shallow tunnel under unsymmetrical pressure based on stochastic medium theory. *J. Railw. Eng. Soc.* **2017**, *34*, 70–76.
7. Li, J. Construction technique for a mountain tunnel portal without slope cutting in steep terrain. *Mod. Tunn. Technol.* **2013**, *50*, 158–163.
8. Shi, Y.; Li, J.; Li, W.; Zhou, X. Construction mechanics of tunnel with super-large cross-section and its dynamic stability. *J. Shanghai Jiaotong Univ.* **2015**, *49*, 1023–1029.

9. Xue, X.H.; Sun, Z.J.; Su, Z.M.; Song, F. Study on Mechanical Properties of Compound-umbrella Arch in Bias Tunnel Entrance. In *Applied Mechanics and Materials*; Trans Tech Publications Ltd.: Zurich, Switzerland, 2013; Volume 438, pp. 987–990.
10. Wu, D.; Li, W.; Xie, B.; Wang, W.; Pan, W. Study on the Spatial Effect of Construction Disturbance in Tunnel Construction with Steep Slope Bias Pressure and Small Clear Distance. *Railw. Eng. Sci.* **2016**, *13*, 906–913.
11. Wang, Y.; Li, Z.; Yu, L.; Zou, C.; Wang, L. Research on the vertical earth pressure at the top of the railway cutting-type Mingdong. *Railw. Stand. Des.* **2018**, *62*, 104–109.
12. Fu, H.; Li, K.; Wang, H.; Zhang, J.; Huang, Z. Prediction of settlement of shallow-buried biased tunnels based on random medium theory. *Chin. J. Railw. Eng.* **2017**, *34*, 70–76.
13. Ministry of Transport of the People's Republic of China. *JTG/T3660—2020 Code for Construction Technique of Highway Tunnel*; China Communications Press: Beijing, China, 2020.
14. Bai, W.; Yao, H.; Hu, X. Judgment method and design and construction measures of terrain biased tunnel. *Road Constr. Mach. Constr. Mech.* **2016**, *33*, 76–79.
15. Zheng, H. Research on the influence of different terrain conditions on the bias pressure of tunnels with different elevations and small clear distances. *Constr. Technol.* **2018**, *47*, 8–11, 24.
16. Dai, S.; Zuo, T.; Hou, J.; Wan, Y. Analysis of surface treatment measures for terrain biased tunnels. *Sci. Technol. Eng.* **2020**, *20*, 3308–3314.
17. Xu, T.; Yan, S.; Wang, F.; Cheng, J. Study on the influence of stratum dip angle on the settlement of shallow buried eccentric pressure tunnel vault. *Railw. Stand. Des.* **2019**, *63*, 137–140, 149.
18. Liu, F.; Yu, Y.; Wang, Q.; Luo, Y. A coupled smoothed particle hydrodynamic and finite particle method: An efficient approach for fluid-solid interaction problems involving free-surface flow and solid failure. *Eng. Anal. Bound. Elem.* **2020**, *118*, 143–155. [[CrossRef](#)]
19. Zhang, J.; Li, S.; Zhang, Q.; Zhang, X.; Li, P.; Wang, D.; Weng, X. Mud inrush flow mechanisms: A case study in a water-rich fault tunnel. *Bull. Eng. Geol. Environ.* **2019**, *78*, 6267–6283. [[CrossRef](#)]
20. Wang, F.M.; Li, X.L.; Zhong, Y.H.; Chen, X.G. Stability Analysis of Tunnel Surrounding Rock Based on Coupled Fluid-Solid Theory. In *Applied Mechanics and Materials*; Trans Tech Publications Ltd.: Zurich, Switzerland, 2011; Volume 90, pp. 1900–1903.
21. Hwang, R.H.; Yang, T.H.; Sun, P.F. Influence of anisotropic rock on tunnel stability with consideration of fluid-solid coupling. In *Applied Mechanics and Materials*; Trans Tech Publications Ltd.: Zurich, Switzerland, 2011; Volume 90, pp. 2101–2107.
22. Zhang, Q.; Shao, C.; Wang, H.Y.; Jiang, B.S.; Jiang, Y.J.; Liu, R.C. A fully coupled hydraulic-mechanical solution of a circular tunnel in strain-softening rock masses. *Tunn. Undergr. Space Technol.* **2020**, *99*, 103375. [[CrossRef](#)]
23. Zhou, W.; Liao, S.; Men, Y. A fluid-solid coupled modeling on water seepage through gasketed joint of segmented tunnels. *Tunn. Undergr. Space Technol.* **2021**, *114*, 104008. [[CrossRef](#)]
24. Schrefler, B.A.; Codina, R.; Pesavento, F.; Principe, J. Thermal coupling of fluid flow and structural response of a tunnel induced by fire. *Int. J. Numer. Methods Eng.* **2011**, *87*, 361–385. [[CrossRef](#)]
25. Guo, J.-Q.; Luo, Y.-B.; Chen, F.; Luo, Y.-B.; Liu, Q. Water inrush criterion and catastrophe process of a karst tunnel face with non-persistent joints. *China J. Highw. Transp.* **2018**, *31*, 118.
26. Karami, M.; Kabiri-Samani, A.; Nazari-Sharabian, M.; Karakouzian, M. Investigating the effects of transient flow in concrete-lined pressure tunnels, and developing a new analytical formula for pressure wave velocity. *Tunn. Undergr. Space Technol.* **2019**, *91*, 102992. [[CrossRef](#)]
27. Karakouzian, M.; Nazari-Sharabian, M.; Karami, M. Effect of overburden height on hydraulic fracturing of concrete-lined pressure tunnels excavated in intact rock: A numerical study. *Fluids* **2019**, *4*, 112. [[CrossRef](#)]
28. Simanjuntak, T.D.Y.F.; Marence, M.; Mynett, A.E.; Schleiss, A.J. Pressure tunnels in non-uniform in situ stress conditions. *Tunn. Undergr. Space Technol.* **2014**, *42*, 227–236. [[CrossRef](#)]
29. Lee, S.W.; Jung, J.W.; Nam, S.W.; Lee, I.M. The influence of seepage forces on ground reaction curve of circular opening. *Tunn. Undergr. Space Technol.* **2007**, *22*, 28–38. [[CrossRef](#)]
30. Hwang, J.H.; Lu, C.C. A semi-analytical method for analyzing the tunnel water inflow. *Tunn. Undergr. Space Technol.* **2007**, *22*, 39–46. [[CrossRef](#)]
31. Ma, S.; Chen, W.; Zhao, W. Mechanical properties and associated seismic isolation effects of foamed concrete layer in rock tunnel. *J. Rock Mech. Geotech. Eng.* **2019**, *11*, 159–171. [[CrossRef](#)]
32. Kaselouris, E.; Nikolos, I.K.; Orphanos, Y.; Bakarezos, M.; Papadogiannis, N.A.; Tatarakis, M.; Dimitriou, V. Elastoplastic study of nanosecond-pulsed laser interaction with metallic films using 3D multiphysics fem modeling. *Int. J. Damage Mech.* **2016**, *25*, 42–55. [[CrossRef](#)]
33. Yang, C.; Hu, Z.X.; Huang, D.; Guo, F. Failure Mechanism of Primary Support for a Shallow and Asymmetrically Loaded Tunnel Portal and Treatment Measures. *J. Perform. Constr. Facil.* **2020**, *34*, 04019105. [[CrossRef](#)]
34. Zhang, Z.; Zhao, C.; Peng, L.; Zhang, X.; Lei, M. Research on the stability of shallow-buried large cross-section tunnel by construction method conversion. *Front. Earth Sci.* **2022**, *37*. [[CrossRef](#)]
35. *FLAC3D*; Fast Lagrangian Analysis of Continua in 3 Dimensions. ITASCA Consulting Group, Inc.: Minneapolis, MN, USA, 2009.
36. *JTG D70*; Industry Standard of the People's Republic of China. Code for Design of Road Tunnel. Communication Press: Beijing, China, 2004. (In Chinese)